Genes & Diseases (2023) 10, 1114–1129

Available online at www.sciencedirect.com

ScienceDirect

journal homepage: www.keaipublishing.com/en/journals/genes-diseases

FULL LENGTH ARTICLE

The miR-21-5p enriched in the apoptotic bodies of M2 macrophage-derived extracellular vesicles alleviates osteoarthritis by changing macrophage phenotype

Leilei Qin [a,b], Jianye Yang [a,b], Xudong Su [a,b], Xilan li [c], Yiting Lei [a,b], Lili Dong [a,b], Hong Chen [a,b], Cheng Chen [a,b], Chen Zhao [a,b], Huan Zhang [a,b], Jun Deng [c,**,#], Ning Hu [a,b,***,#], Wei Huang [a,b,*,#]

[a] *Department of Orthopaedics, The First Affiliated Hospital of Chongqing Medical University, Chongqing 400016, China*
[b] *Orthopedic Laboratory of Chongqing Medical University, The First Affiliated Hospital of Chongqing Medical University, Chongqing 400016, China*
[c] *Institute of Burn Research, Southwest Hospital, State Key Lab of Trauma, Burn and Combined Injury, Army Medical University, Chongqing 400038, China*

Received 16 May 2022; received in revised form 9 August 2022; accepted 28 September 2022
Available online 5 October 2022

KEYWORDS
Apoptotic body;
Extracellular vesicles;
Macrophage phenotype switch;
MicroRNA-21;
Osteoarthritis

Abstract Macrophages (Mφs) play a crucial role in the pathological progression of osteoarthritis (OA) by regulating inflammation and tissue repair. Decreasing pro-inflammatory M1-Mφs and increasing anti-inflammatory M2-Mφs can alleviate OA-related inflammation and promote cartilage repair. Apoptosis is a natural process associated with tissue repair. A large number of apoptotic bodies (ABs), a type of extracellular vesicle, are produced during apoptosis, and this is associated with a reduction in inflammation. However, the functions of apoptotic bodies remain largely unknown. In this study, we investigated the role of M2-Mφs-derived

* Corresponding author. Department of Orthopaedics, The First Affiliated Hospital of Chongqing Medical University, Chongqing 400016, China.
** Corresponding author. Institute of Burn Research, Southwest Hospital, State Key Lab of Trauma, Burn and Combined Injury, Army Medical University, Chongqing 400038, China.
*** Corresponding author. Department of Orthopaedics, The First Affiliated Hospital of Chongqing Medical University, Chongqing 400016, China.
E-mail addresses: djun.123@163.com (J. Deng), huncqjoint@yeah.net (N. Hu), huangwei68@263.net (W. Huang).
Peer review under responsibility of Chongqing Medical University.
# These authors contributed equally to this work and should be considered as equal corresponding authors.

https://doi.org/10.1016/j.gendis.2022.09.010

apoptotic bodies (M2-ABs) in regulating the M1/M2 balance of macrophages in a mouse model of OA. Our data show that M2-ABs can be targeted for uptake by M1-Mφs, and this reprograms M1-to-M2 phenotypes within 24 h. The M2-ABs significantly ameliorated the severity of OA, alleviated the M1-mediated pro-inflammatory environment, and inhibited chondrocyte apoptosis in mice. RNA-seq revealed that M2-ABs were enriched with miR-21—5p, a microRNA that is negatively correlated with articular cartilage degeneration. Inhibiting the function of miR-21—5p in M1-Mφs significantly reduced M2-ABs-guided M1-to-M2 reprogramming following *in vitro* cell transfection. Together, these results suggest that M2-derived apoptotic bodies can prevent articular cartilage damage and improve gait abnormalities in OA mice by reversing the inflammatory response caused by M1 macrophages. The mechanism underlying these findings may be related to miR-21-5p-regulated inhibition of inflammatory factors. The application of M2-ABs may represent a novel cell therapy, and could provide a valuable strategy for the treatment of OA and/or chronic inflammation.

Introduction

Macrophages (Mφs) are innate immune cells present in every tissue, and play a critical role in the initiation, maintenance and resolution of inflammation, leading to tissue damage or repair.[1,2] The effects of Mφs are associated with the high degree of heterogeneity and plasticity among the different phenotypes.[3,4] In brief, macrophages activated by specific microenvironmental signals can be broadly divided into two subtypes, classically activated M1-Mφs with pro-inflammatory effects and alternately activated M2-Mφs with anti-inflammatory and tissue repair functions.[5] The polarization (M1 vs. M2) of macrophages is important for the progression and prognosis of inflammatory diseases, and the ratio of M1/M2 Mφs is highly regulated under physiological conditions.[6] However, in some pathological states, the M1-Mφs dominate, triggering and/or accelerating the progression of conditions as diverse as osteoarthritis (OA), inflammatory bowel disease and wound healing.[7]

Therefore, the regulation of macrophages provides a possible strategy for preventing or treating inflammatory diseases. It has previously been demonstrated that a severe M1/M2 imbalance participates in the initiation of OA.[8] Targeted macrophage polarization may represent a promising treatment for OA. Reprogramming pro-inflammatory M1-Mφs into anti-inflammatory M2-Mφs can decrease synovial inflammation and cartilage destruction in models of OA.[9] Notably, the maintenance of macrophage phenotypes is driven by genetic/epigenetic signals and is influenced by environmental signals.[10,11]

It is well known that extracellular vesicles with an intact membrane structure are released by cells.[12] These tiny vesicles carry genetic materials from their cells of origin, including microRNA, mRNA, DNA and proteins, all of which can play important roles in cell communication and signaling.[13—15] There are three main subtypes of extracellular vesicles: exosomes, micro-vesicles, and apoptotic bodies.[16] Apoptotic bodies, the product of programmed apoptosis, contain bioactive substances and can be specifically recognized by macrophages via the "eat-me" signal (calreticulin) on their surfaces.[17,18] In addition, previous studies have observed that the endocytosis of apoptotic cells (apoptotic bodies) by macrophages contributes to tissue repair and the regression of inflammation.[19] Whether this reduction in inflammation and enhanced tissue repair are related to phenotypic changes after the uptake of apoptotic bodies by macrophages remains unclear.

In this study, we found that M1-Mφs can be effectively converted to M2 Mφ after phagocytosis of M2-derived apoptotic bodies. Moreover, the reprogrammed M2 Mφ expressed specific markers of M2-Mφs and secreted anti-inflammatory cytokines. Subsequently, M2-derived apoptotic bodies (M2-ABs) were injected into the knees of a mouse model of OA generated by anterior cruciate ligament transection (ACLT). *In vivo*, there was Mφ phenotypic conversion of M1 to M2, and this successfully alleviated the progression of OA (Fig. 1A).

Material and methods

Cell culture

The primary macrophages were derived from bone marrow-derived macrophages (BMDM) of C57BL/6 mice. To put it simply, bone marrow from the femur and tibia was obtained, washed and filtered to form a single-cell suspension, which was maintained for 7 days in RPMI-1640 (Gibco) medium supplemented with 10% fetal bovine serum (Gibco), 1% penicillin/streptomycin (Invitrogen, USA) and 10 ng/mL M-CSF (PeproTech, USA). M1 was obtained by stimulation of 40 ng/mL IFN-γ (Peprotech) for 48 h. For M2 activation, cells were treated with 20 ng/mL IL-4 (Peprotech) for 48 h. For the analysis of phagocytosis experiment, NIH-3T3 fibroblasts and HUVECs were obtained from Procell Life Science & Technology Co. Ltd (Wuhan, China).

Chondrocytes were derived from male C57BL/6 mice. The articular cartilage was separated and cut into 1 mm fragments. The chondrocytes were digested with 0.25% trypsin and 0.2% collagenase at 37 °C for 30 min and 5 h, respectively. The cells were filtered through a 70 μm cell filter and rinsed with sterile phosphate-buffered saline

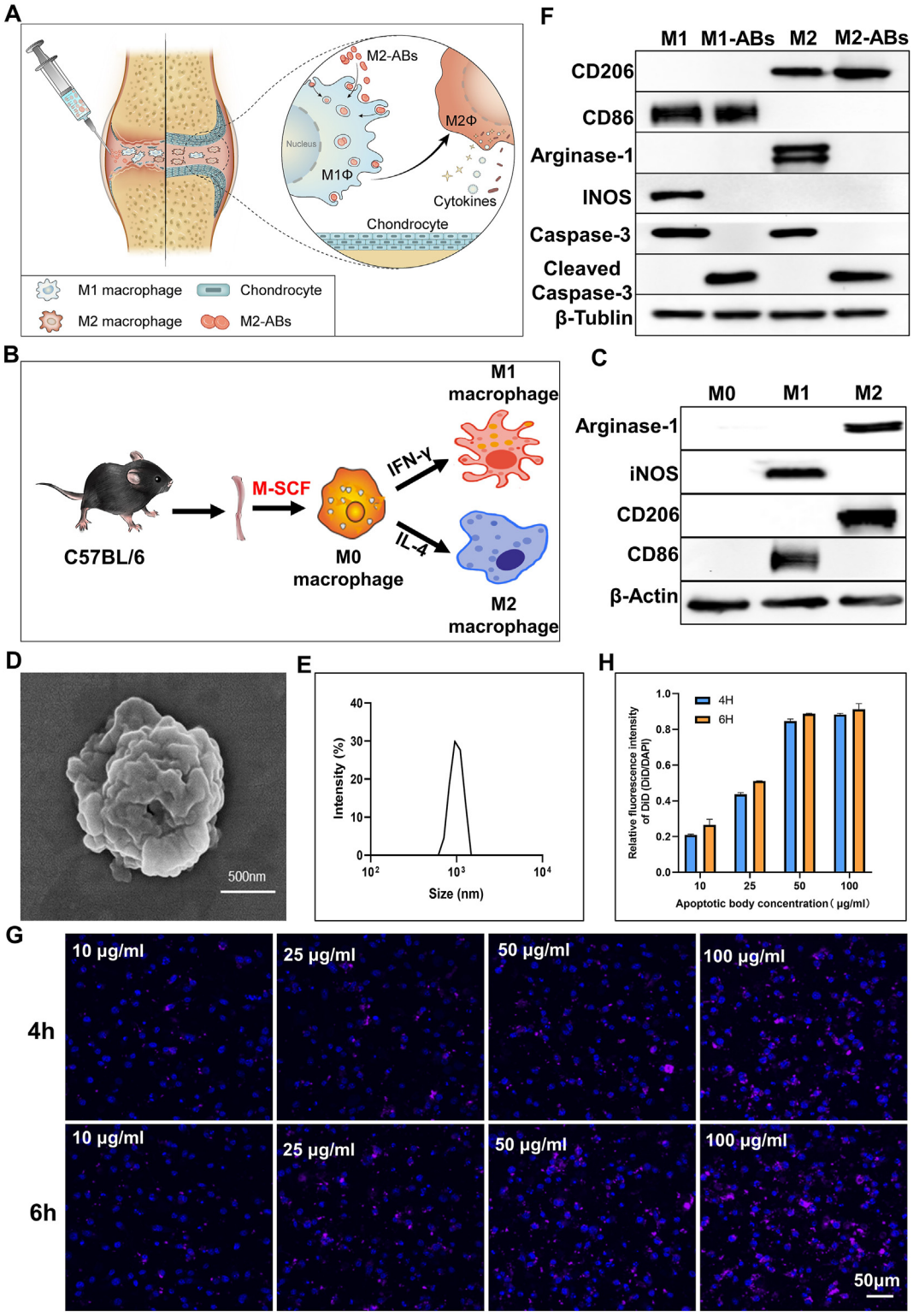

Figure 1 Establishment of M1 and M2 Mφs and characterization of Mφ-ABs. **(A)** Schematic illustration of apoptotic bodies-guided macrophage reprogramming. M2 Mφ-derived apoptotic bodies (M2-ABs) can trigger the switch of M1 to M2 Mφs transformation and alleviate the progression of osteoarthritis. **(B)** Schematic diagram of obtaining M1 and M2 Mφs. **(C)** Western blot analysis showed the expression of Mφ markers 24 h after polarization. **(D)** Representative SEM image of ABs. Scale bar, 500 nm. **(E)** Size distribution of ABs measured by DLS. **(F)** Western blot analysis specific protein markers of Mφs and Mφs-ABs. **(G)** Confocal images of M1 Mφs incubation with 10, 25, 50, and 100 μg/mL of DiD-labeled M2-ABs in 4 or 6 h, respectively (Red: DiD-labeled M2-ABs; Blue: cell nuclear). Scale bars, 50 μm. **(H)** Relative fluorescence intensity of DiD-labeled M2-ABs internalized in M1 Mφs.

(PBS) 3 times. The collected chondrocytes were then cultured in a DMEM (Gibco) dish at 37 °C and 5% CO_2. The medium was changed every 2−3 days, and only primary or subgeneration chondrocytes were used during the experiment.

Isolation and characterization of ABs derived from BMDM

Macrophages were starved in serum-free medium for 24 h, and then treated with staurosporine (0.5 μM) for 4 h to induce apoptosis. The culture medium was collected and centrifuged at 50 g for 5 min to remove the cells and debris. After two repetitions, the supernatant was further centrifuged for 1000 g (10 min) to concentrate ABs into particles, which were then resuspended with 1 × PBS and stored at −80 °C for subsequent experiments. The protein concentration was measured using the BCA protein Detection Kit. DLS analysis was performed using a Zetasizer Nano ZSE (Malvern, UK). The morphology of the ABs was observed by SEM (Hitachi, Japan). Western blotting was performed to characterize the protein constitution of the ABs.

ABs labeling and cell phagocytosis

ABs derived from Mφs were labeled with a membrane labeling dye (1′-dioctadecyl-3,3,3′,3′-tetramethylindodicarbocyanine, DiD) (Thermo Fisher Scientific) according to the manufacturer's protocol. The ABs were incubated in a 5 μg/mL DiD staining solution at 37 °C for 30 min, washed with PBS, and centrifuged at 3000 g for 30 min for two consecutive times. Ultrafiltration tube (300 kDd, Sigma Aldrich) was used to remove the unattached dye. The cells were inoculated in 35 mm confocal dish with a density of 1×10^6, co-cultured with DiD labeled ABs in different concentrations at 37 °C for 4 or 6 h, and then observed with a confocal microscope (Olympus SpinSR10, Japan).

Effects of ABs on cell viability

The cytotoxicity of ABs with M1 and M2 Mφs were evaluated using Cell Counting Kit-8 (CCK-8, Beyotime Bio-Tech, China). Cells (1×10^4 cells well-1) were seeded in 96-well plates and cultured in RPMI-1640 overnight. Then, M2-ABs (0, 5,10, 15, 25, 50, 100 and 200 μg/mL) were added into the cells and incubated for another 24 h in a humidified atmosphere with 5% CO_2 at 37 °C. Then, the cells were washed with PBS and incubated with 10% CCK-8 solution for 2 h at 37 °C. Finally, the absorbance was measured at 450 nm using a microplate reader (Bio-Rad, Hercules, CA, USA).

Western blot analysis

Protein concentration of cells and ABs was determined by BCA protein assay. The same amount of total protein was separated in 4%−10% SDS-PAGE and transferred to the PVDF membrane. The proteins transferred to the membrane were blocked at room temperature with 5% skim milk for 60 min, followed by overnight incubation with primary antibodies at 4 °C. Then, after washing with TBS-T, the membrane was incubated for 2 h at room temperature with secondary horseradish peroxidase-conjugated goat anti-rabbit IgG. The protein bands were visualised with enhanced chemiluminescence (Thermo Fisher Scientific, iBright FL1500, USA). The antibodies used in this procedure are as follows: β- Tubulin (CST, #2146, 1:1000), β-actin (CST, #8457, 1:1000), CD86 (CST, #91882, 1:1000), iNOS (CST, #13120, 1:1000), CD206 (CST, #24595,1:1000), Arginase-1 (CST, #93668, 1:1000), Caspase-3 (CST, #9662,1:1000), Cleaved Caspase-3 (CST, #9664,1:1000).

Quantitative real-time polymerase chain reaction (q-PCR)

Total RNA was isolated using Trizol reagent (Life Technologies). Single-stranded cDNA was prepared from 1 μg of total RNA using reverse transcriptase with oligo-dT primer according the manufacturer's instructions (Promega, USA). The primers used are listed in Table S1. Values were normalized to GAPDH mRNA levels and calculated by $2^{-\Delta\Delta Ct}$.

Immunocytochemistry

The cultured cells were fixed in 4% paraformaldehyde for 10 min and then washed three times with PBS. They were then permeated in 0.25% Triton X-100 (Sigma−Aldrich) for 5 min, followed by washing with PBS three times. The PBST solution containing 1% BSA was blocked for 1 h and then added with primary antibody at 4 °C overnight. The cells were washed three times with PBST and then the secondary antibodies were incubated in the dark for 1 h at room temperature. After three PBST washes, 4′,6- diamidino- 2-phenylindole (DAPI) staining was performed. Images were captured using a confocal microscope (Olympus SpinSR10, Japan). The antibodies used in this procedure are as follows: iNOS (CST, #13120, 1:200), CD206 (CST, #24595,1:200), Arginase-1 (CST, #93668, 1:200), Alexa Fluor 488 (Anti-Rabbit IgG ($H + L$), Beyotime, 1:1000), Alexa Fluor 647 (Anti-Rabbit IgG ($H + L$), Beyotime, 1:1000).

Flow cytometry

The stained macrophages were analyzed by flow cytometry (Thermo Fisher Scientific, Attune NxT, USA). Staining and analysis of cells according to operator's manual and reagent instructions. The antibodies used in this procedure are as follows: CD11b-FITC (Biolgend, #101206, USA), PE-CD86 (Biolgend, #105008, USA), Brilliant Violet 421-F4/80 (Biolgend, #123132, USA), Brilliant Violet 650-CD206 (Biolgend, #141723, USA). All of the data were analyzed with FlowJo software (Tree Star).

Cytokine measurements in reprogrammed M2 mφs (RM2)

The cells were cultured in serum-free medium for 24 h, followed by a 500 μL medium collection. The samples were processed using the Bio-Plex mouse cytokine 23-Plex panel

arrays (Bio-Rad Laboratories, Hercules, CA, USA) and detected using the Bio-Plex Protein Array System (Bio-Rad Laboratories) according to the manufacturer's instructions. The concentrations were calculated using the function: Relative concentration cytokine concentration/total protein concentration.

Effect of RM2 on chondrocyte proliferation

Primary chondrocytes were plated in a six-well culture plate (Corning, PET, 0.4 μm, USA) at a density of 2×10^5 cells per well in a fresh culture medium. Cells were incubated at 37°C and 5% CO_2 overnight to allow the formation of a confluent monolayer at 70% confluence. Subsequently, M1, M2, or RM2 were added to each well at a density of 2.5×10^5 cells per well. After 24 h of co-culture, the upper compartment was abandoned and the proliferative activity of EDU cells was analyzed. EdU incorporation was performed using the BeyoClick™ EdU Cell Proliferation Kit with Alexa Fluor 488 (Beyotime; Shanghai, China) according to the manufacturer's protocol. Incubate with the same volume of EdU solution at 37 °C for 2 h. Cells were fixed with 4% paraformaldehyde for 15 min, permeabilized with 0.3% TritonX-100 for 15 min, and incubated with 500 μL of click-reactive solution for 30 min. All nuclei were stained with Hoechst 33,342 and the percentage EdU-positive/Hoechst-positive was calculated. Images were captured using a fluorescence microscope (Olympus, IX71, Japan).

RNA sequencing (RNA-seq) analysis

Total RNAs were extracted from M2 - derived apoptotic bodies using TRIzol reagent (Invitrogen, cat. No. 15596026) following the methods by Chomczynski et al (https://doi.org/10.1006/abio.1987.9999). DNA digestion was carried out after RNA extraction by DNaseI. RNA quality was determined by examining A260/A280 with NanodropTM OneCspectrophotometer (Thermo Fisher Scientific Inc). RNA integrity was confirmed by 1.5% agarose gel electrophoresis. Qualified RNAs were finally quantified by Qubit 3.0 with QubitTM RNA Broad Range Assay kit (Life Technologies, Q10210). Two μg total RNAs were used for stranded RNA sequencing library preparation using Ribo-off rRNA Depletion Kit (Mouse) (Catalog No. MRZG12324, Illumina) and KC-DigitalTM Stranded mRNA Library Prep Kit for Illumina® (Catalog No. DR08502, Wuhan Seqhealth Co., Ltd. China) following the manufacturer's instruction. The kit eliminates duplication bias in PCR and sequencing steps, by using a unique molecular identifier (UMI) of 8 random bases to label the pre-amplified cDNA molecules. The library products corresponding to 200—500 bps were enriched, quantified, and finally sequenced on NovaSeq 6000 sequencer (Illumina) with PE150 model.

MicroRNA transfection

Macrophages were transfected with miR-21—5p inhibitor and inhibitor negative control (NC) (Shanghai GenePharma Co. Ltd.) using Lipofectamine 3000 (cat. No. L3000015; Invitrogen: Thermo Fisher Scientific, Inc.) at a final concentration of 100 nM, and the same conditions were applied for each transfection experiment. Transfection was evaluated under a fluorescence microscope at 12 h and further experiments were continued at 24 h. The sequences of inhibitor and negative controls were as follows: miR-21—5p inhibitor, CY5-5′-UCAACAUCAGUCUGAUAAGCUA-3′; and inhibitor negative control, 5′-UCAACAUCAGUCUGAUAAGCUA-3′.

Distribution of ABs *in vivo*

We fluorescently labeled ABs according to the instructions of fluorescent reagent (Cyanine 7 NHS Ester Cy7 NHS, #MX4669-1 MG, China). *In vivo* fluorescence analysis was performed on C57BL/6 mice. All animal experiments were performed in accordance with the International Guide for the Care and Use of Laboratory Animals and approved by the Research Ethics Committee of the First Affiliated Hospital of Chongqing Medical University (2021—526). Injection of PBS or ABs (10 μg per 10 μL) into mouse knee joint ($n = 5$). The fluorescence intensity was measured by *in vivo* imaging system (AniView100, BLT, Guangzhou, China). The fluorescence intensity of tumor region of interest (ROIs) was quantitatively analyzed using AniView software (BLT, Guangzhou, China).

Mice knee OA model induced by anterior cruciate ligament transection (ACLT)

20 male mice (8 weeks old) were established as osteoarthritis models according to previous research methods.[20] These mice were randomly divided into four groups of 5 mice each. The mice were treated with the sham operation as the control group. The sham operation was performed by only opening the joint capsule and then suturing the incision. The other three groups of mice were anesthetized, with the joint cavity opened and the anterior cruciate ligament (ACL) transected, followed by delamination and closure of the skin. After surgery, each group was injected with 10 μl equal volume of PBS, M1-ABs (10μg/10 μL) and M2-ABs (10μg/10 μL) in the joint cavity for 5 consecutive weeks, once a week.

Evaluations with micro-CT scanning

After 5 weeks of treatment, the mice were sacrificed and the obtained knee joints were immobilized with 4% paraformaldehyde (pH 7.4). Micro-CT (Viva CT80; Scanco, Zurich, Switzerland) was used to scan the knee tissue with a resolution of 10 μm. We defined the region of interest (ROI) as covering the entire subchondral bone of the tibial plateau. Three-dimensional structural parameters analyzed included bone volume (BV), bone volume/total tissue volume (BV/TV), and trabecular number (Tb. *n*), thickness (Tb. Th) and separation (Tb. Sp).

Histological analysis

The sample was decalcificated in 10% EDTA and then embedded in paraffin. Sagittal sections (4 μm thick) were stained with hematoxylin-eosin (H&E) and Safranin O-fast green (S&F). Histologic scoring was performed by two

blinded observers using a modified Mankin scoring system.[21] Immunohistochemistry and immunofluorescence staining were accomplished with antibodies against CD86 and CD206 (CST; dilution 1:200), Images were captured using a Zeiss Axio Imager light microscope. The relative expression of aggrecan was quantified by ImageJ software.

Statistical analysis

All data were shown as the mean ± standard deviation. All groups were compared with a student *t*-test or one-way analysis of variance, and *P*-values less than 0.05 were considered statistically significant. Graph analysis was performed using GraphPad Prism 9.0 (GraphPad Software, USA).

Results

Identification of M1 and M2 mφs and characterization of macrophage-derived apoptotic bodies

To avoid differences between mouse strains and genders, all mononuclear macrophages were obtained from 6-to-8-week-old male C57BL/6 mice. We differentiated primary monocytes from mouse bone marrow-derived hematopoietic stem cells (HSCs) and activated Mφs with different functional phenotypes, followed by the extraction of macrophage-derived apoptotic bodies from the classically activated M1-Mφs (M1-ABs) and alternately activated M2-Mφs (M2-ABs) (Fig. 1B).

In brief, bone marrow-derived mononuclear cells isolated from mouse tibia were incubated *in vitro* with monocyte-colony stimulating factor (M-CSF) for 7 days to differentiate the cells into macrophages.[22] During the culture process, macrophage precursor cells adhered to the wall were activated, allowed to proliferate, and gradually differentiated into mature macrophages Mφs (M0). Fluorescence-activated cell sorting (FACS) analyses showed that more than 98% of HSCs differentiated into mature CD11b and F4/80 double-positive M0 cells (Fig. S1). We further stimulated the unpolarized M0 with IFN-γ and IL4, respectively, and 24 h later[23] flow cytometry showed that more than 95% of the M0 cells had been polarized to M1 ($F4/80^+$ and $CD86^+$) and M2 ($F4/80^+$ and $CD206^+$) Mφs (Fig. S2). Western blot analysis showed that the M0 cells clearly started to express the representative marker proteins of M1 (CD86 and iNOS) and M2 (Arginase and CD206) Mφs under different stimulus conditions (Fig. 1C). In addition, the classically activated M1 and alternatively activated M2 Mφs showed the typical fried egg and spindle-shaped cell morphology, respectively (Fig. S3).

We induced apoptosis in the M1 and M2 cells by exposing them staurosporine and then obtained apoptotic bodies by differential centrifugation.[24] Scanning electron microscopy (SEM) showed that Mφ-derived ABs were vesicles approximately 1 μm in diameter (Fig. 1D), which was consistent with the dynamic light scattering (DLS) data (Fig. 1E). Both M1-ABs and M2-ABs expressed the same membrane markers (CD86 and CD206) as the source cells, and had high levels of cleaved caspase-3, indicating the successful induction of apoptosis (Fig. 1F). Notably, the typical intracellular proteins (INOS and ARG-1) of the source cells were not detected in either the M1-ABs or M2-ABs, indicating that the apoptotic bodies did not simply transfer donor-specific labeled proteins to the recipient cells (Fig. 1G).

Next, we evaluated the efficiency of the uptake of apoptotic bodies by Mφs (Fig. 1G). The Mφs were cultured with fluorescent dye-labeled apoptotic bodies at concentration gradients of 0−100 μg/mL for 4 or 6 h. The cytotoxicity of the AB was determined by the CCK-8 assay, and the viability remained above 93.7% for both the M1 and M2 Mφs incubated with 100 μg/mL of M2-ABs (Fig. S4). Confocal microscopy showed that the attachment and internalization of apoptotic bodies in M1-Mφs increased in a dose- and time-dependent manner, and the internalization of apoptotic bodies by macrophages tended to be stable when the concentration of apoptotic bodies was 50 μg/mL for 4 h (Fig. 1H). Therefore, the 50 μg/mL concentration of apoptotic bodies was selected to determine whether it is possible to reprogram macrophage phenotypes.

Because we are particularly interested in the uptake of apoptotic bodies by macrophages inside the knee joint, we compared the ability of other types of cells to acquire apoptotic bodies under the same conditions (Fig. S5). As expected, the M1-Mφs demonstrated the greatest uptake of ABs, supporting the possibility that apoptotic bodies might reprogram M1-Mφs *in vivo*.

Evaluation of M2-ABs reprogramming M1 to M2 mφs *in vitro*

To verify whether Mφ-ABs can trigger the reprogramming of Mφs from the pro-inflammatory M1 phenotype to the anti-inflammatory M2 phenotype, we first incubated M1-Mφs with 50 μg/mL M1-ABs or M2-ABs for 24 h (Fig. S6). Western blot analyses suggested that M1-ABs enhanced the polarization of M1. Of note, the expression of arginase was significantly increased in the M1-Mφs incubated with M2-ABs.

We next examined the time-dependent changes associated with incubating 50 μg/mL M2-ABs to reprogram M1-Mφs to the M2 phenotype. An immunocytochemical (ICC) analysis showed that with the increase in the incubation time, the expression of iNOS gradually decreased. After 48 h, the expression of iNOS had almost completely disappeared from the cells, and the expression of arginase was strongly induced (Fig. 2A). Western blot and RT-qPCR experiments demonstrated that with the increase in incubation time, the protein expression levels of arginase and CD206 in the M1-Mφs gradually increased and reached a maximum after 48 h (Fig. 2B, D).

To accurately quantify the extent to which M2-ABs guided M1-Mφ reprogramming, a flow cell measurement method was used to compare the CD206 positive rates of classically activated M1-Mφs and the M1-Mφs incubated with 50 μg/mL M2-ABs for different periods of time (Fig. 2E). A flow cytometry analysis showed that the proportion of M1 reprogrammed to M2 reached 40.6% after 24 h of incubation with M2-ABs, and this significantly increased to 79.0% after 48 h and stabilized at 81.5% after 72 h. These

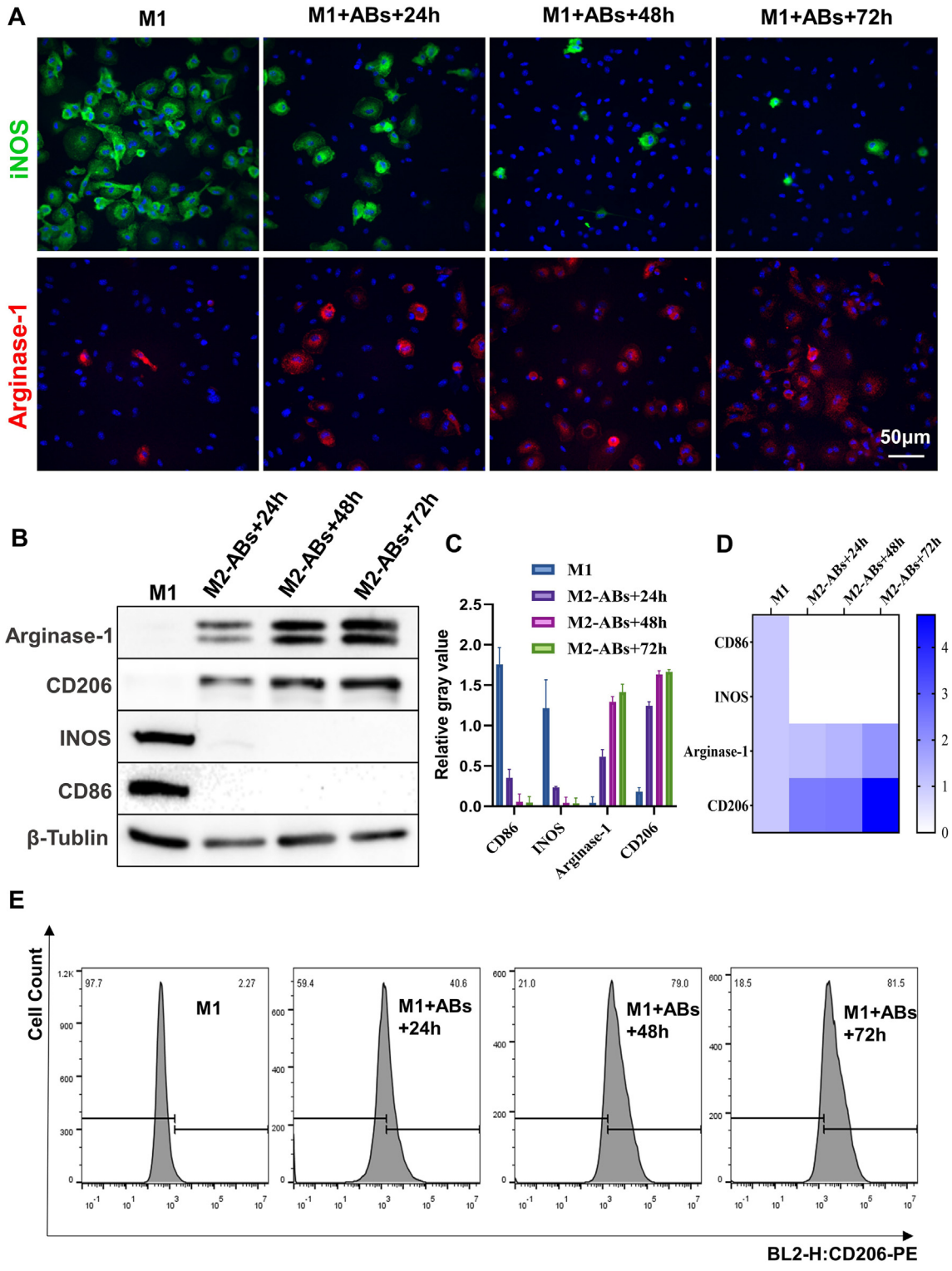

Figure 2 M2-ABs guided reprogramming of M1 Mφs to M2 Mφs. **(A)** Immunostaining of iNOS and Arginase in M1 Mφs after 24 h, 48 h and 72 h incubation with 50 μg/mL of M2-ABs, respectively. **(B)** Western blot analysis of M1 Mφs treated with 50 μg/mL of M2-ABs over time. **(C)** Relative gray value of M1 and M2 Western blot markers in Mφs. **(D)** Heat map for expression analysis (using RT-qPCR) of M1 and M2 macrophages marker genes ($n = 3$). **(E)** FACS histogram showed reprogramming efficiency of M1 Mφs treated with 50 μg/mL of M2-ABs over time.

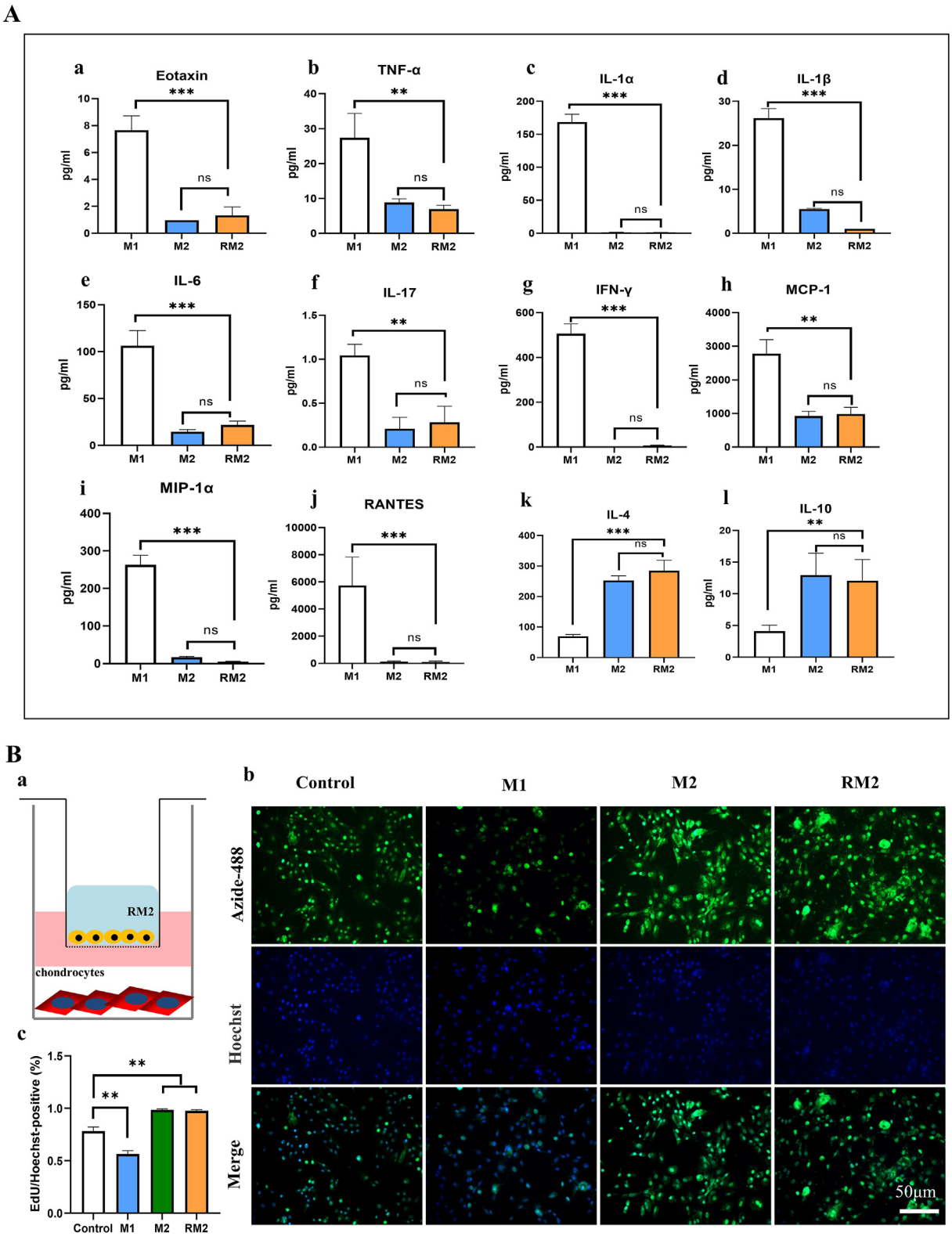

Figure 3 *In vitro* anti-inflammatory and chondrocyte protective effects of RM2 Mφs. **(A)** The concentrations of macrophage serum-free medium cytokines were determined using the Bio-Plex mouse cytokine 23-Plex panel. **(B) a.** Schematic diagram of RM2 co-culture with chondrocytes; **b.** EdU proliferation assays of chondrocytes exposed to classically activated M1-Mφs, alternatively activated M2-Mφs and RM2 for 24 h were performed; **c.** EdU positive fluorescence intensity analysis. ***$P < 0.001$, **$P < 0.01$, *$P < 0.05$.

results indicate that the classically activated M1-Mφs can be successfully reprogrammed into M2 Mφs by a M2-Abs-guided phenotypic switch.

Evaluation of the *in vitro* anti-inflammatory and cartilage protective effects of reprogrammed M2-Mφs (RM2)

Although the above findings indicated that M2-ABs can guide the transition of M1- Mφs to the M2 phenotype (Fig. 2), the ability of the reprogrammed M2-Mφs (RM2) to produce anti-inflammatory cytokines and protect cartilage is unknown. To address these questions, we first evaluated the changes in the secretion of anti-inflammatory and pro-inflammatory cytokines by RM2 and alternately activated M2-Mφs in serum-free medium (Fig. 3A), and then further analyzed the effects of RM2 on the proliferation of chondrocytes (Fig. 3B).

The Bio-plex system was used to analyze the levels of certain cytokines and chemokines in the supernatants of various cell types. The expression levels of proinflammatory cytokines and chemokines such as interleukin-1α/β (IL-1α/β), IL-6, IL-17, Eotaxin, TNF-α, IFN-γ, MCP-1, MIP-1α and RANTES were significantly reduced in both the RM2 and M2-Mφs compared with M1-Mφs (Fig. 3A, a—j). Interestingly, the levels of anti-inflammatory cytokines, such as IL-4 and IL-10, were significantly elevated in the supernatants of RM2 and M2-Mφs, with no significant difference found between RM2 and M2-Mφs (Fig. 3A, k—l).

Chondrocytes achieve satisfactory proliferative activity within 24 h after plating.[25] Therefore, different macrophage populations were co-cultured with chondrocytes in a trans-well chamber for 24 h, and the difference in the proliferation of chondrocytes was detected by the EDU-488 cell proliferation activity kit (Fig. 3B). Compared with the classically activated M1-Mφs, the RM2 and alternatively activated M2-Mφs significantly promoted chondrocyte proliferation (Fig. 3B, b—c) These results further support the idea that local M1-Mφs can be reprogrammed to M2-Mφs, and this may prevent or reduce the progression of osteoarthritis.

M2-ABs drive M1-Mφs reprogramming to M2-Mφs via micro-RNA(s)

Extracellular vesicles can influence the function of recipient cells by delivering miRNAs to regulate gene expression at the post-transcriptional level.[26] Therefore, we profiled and quantified the micro-RNAs in M2-ABs. A total of 886 known microRNAs were identified in the miRNA sequencing analysis of RNA purified from M2-Abs. Next, the top 50 known miRNAs detected in M2-Abs were sorted according to the total reading count (Fig. 4A). Interestingly, among the enriched miRNAs, the expression levels of miR-21a-5p, mmu-let-7c-5p, mmu-miR-146 b-5p, miR-223—3p, miR-34a-5p, miR-29a-3p and miR-125 b-5p have been previously reported to actively participate in the polarization of M2 macrophages.[26—29] Subsequently, a fluorescence-labeled miR-21a-5p inhibitor (GenePharma, Shanghai, China) was transfected into M1-Mφs, and the co-localization of the miR-21a-5p inhibitor and macrophages was detected by fluorescence microscopy 24 h after transfection (Fig. 4B). M2-ABs were added to the M1-Mφs already transfected with miR-21a-5p inhibitors, and the effects of the apoptotic bodies on M1-Mφs reprogramming were evaluated by Western blot and flow cytometry analyses 48 h later. Western blotting showed that M1-Mφs-specific proteins could still be detected in the miR-21a-5p inhibitor group, but not the control group (Fig. 4C), suggesting that miR-21a-5p inhibitors significantly affected the function of M2-ABs. Similarly, in a subsequent flow cytometry study, the proportion of M1-Mφs being reprogrammed to M2-Mφs in the miR-21a-5p inhibitor group was only 46.5%, which was significantly lower than that in the other experimental groups (Fig. 4D; Fig. S7).

Effects of M2-ABs on OA induced by *in situ* transformation of M1 phenotype into M2-Mφs

Before exploring the effects of M2-ABs on the progression of OA, we performed real-time fluorescence imaging analyses of the *in vivo* distribution of M2-ABs (Fig. 5). The fluorescence signal of Cy7-N-hydroxysuccinimide (NHS)-labeled ABs remained clearly in the knee for more than 3 days and was reduced gradually over time (Fig. 5A). On day 5 after joint injection, the signal had diminished to less than 10% of the initial value. Since extensive reprogramming was noted by 72 h during co-incubation *in vitro*, this result suggests that the locally injected ABs would have sufficient time to reprogram the M1-Mφs into M2-Mφs. The apoptotic bodies in mice were mainly metabolized in the liver and kidneys (Fig. 5B, C), and the labeled ABs had completely disappeared on day 6 after injection (Fig. S7). Therefore, our data suggest that weekly local treatment could achieve local macrophage reprogramming and avoid the accumulation of ABs in other organs.

It is thought that during the early stages of osteoarthritis, bone loss is associated with increased bone remodeling.[30] A mouse model of OA can be induced by performing ACLT.[31] Thus, to investigate the effects of M2-ABs on the subchondral bone remodeling of OA, we injected M2-ABs into the knee joint after performing ACLT in mice. The μCT results showed that ACLT injury induced significant bone resorption, with increased subchondral osteolysis of the tibia (Fig. 6). Compared with the PBS-treated ACLT group, the M1-Abs-treated group showed more severe bone loss, while the M2-Abs-treated group showed significant knee bone protection and subchondral bone retention, indicating that osteolysis was diminished after M2-ABs were administered *in vivo* (Fig. 6A, B). The BV of subchondral bone in the tibial plateau was 0.05167 mm^3 in the ACLT group, which was significantly ($P < 0.05$) lower than 0.07553 mm^3 of the control group (Fig. 6C). Nonetheless, compared with the PBS-treated ACLT group, the bone volume of the subchondral bone showed a significant decrease ($P < 0.01$) in the M1-Abs group (0.03973 mm^3) and a significant increase ($P < 0.01$) in the M2-ABs group (0.06843 mm^3) (Fig. 6C). The bone-related parameters, including the trabecular bone volume fraction (BV/TV), trabecular separation (Tb.Sp), trabecular number (Tb.*N*)

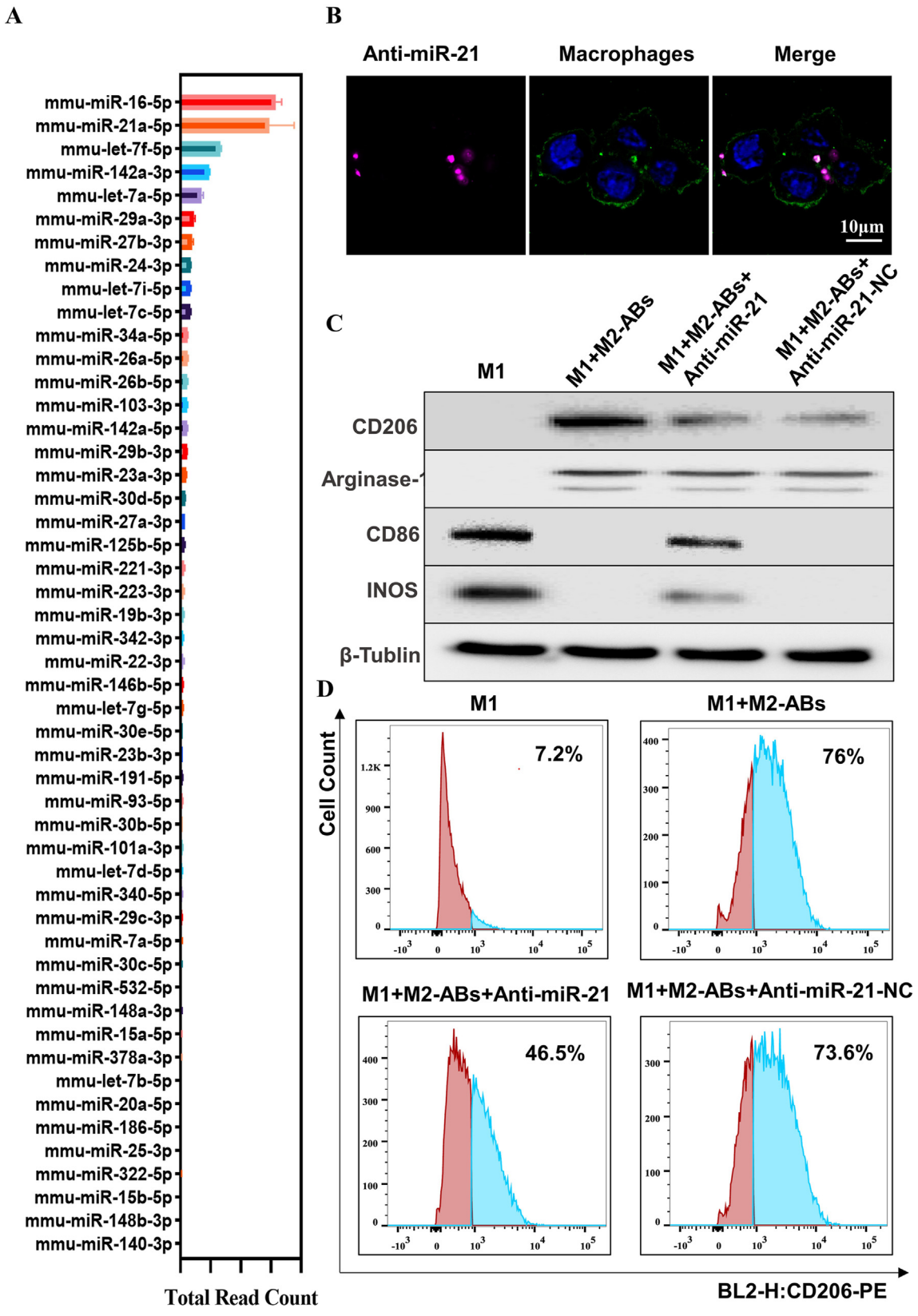

Figure 4 Micro-RNA sequencing (miRNA-seq) analysis and molecular mechanism of M2-ABs. **(A)** Top 50 known miRNAs that were detected in M2-ABs. **(B)** Co-localization of macrophages and miR-21a-5p. **(C)** Western blot analysis of the effect of miR-21a-5p inhibitors on M2-ABs guided M1-Mφs reprogramming to M2-Mφs. **(D)** Flow cytometry (FACS) histogram shows the effect of miR-21a-5p inhibitors on M2-ABs guided M1-Mφs reprogramming to M2-Mφs.

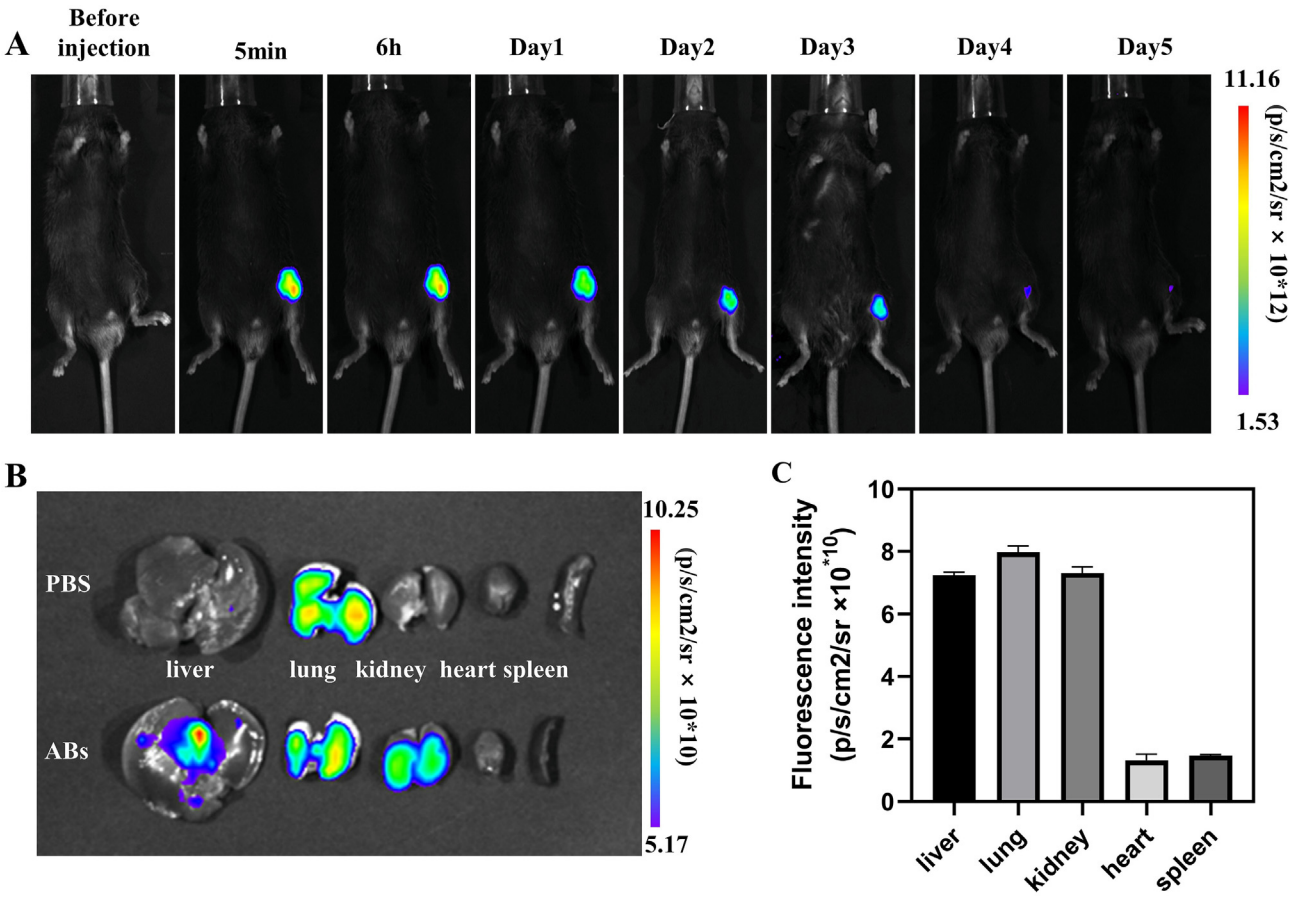

Figure 5 *In vivo* biodistribution of M2-ABs. **(A)** Real-time *in vivo* imaging of Cy7 NHS labeled M2-ABs. The mice were analyzed at the indicated times after knee injection of phosphate-buffered saline (PBS) and 50 μg/μl of M2-ABs. **(B)** *Ex vivo* imaging of major organs at day 3 after mice had been treated with M2-ABs. **(C)** Viscera distribution of fluorescent at day 3 after knee injection of Cy7-NHS labeled M2-ABs.

and trabecular thickness (Tb.Th), also support that M2-ABs play a role in inhibiting bone destruction *in vivo* (Fig. 6C).

In addition to the radiological examinations, the histological changes of the cartilage were also detected. Hematoxylin and eosin (H&E) staining (Fig. 7A) and Safranin O-fast green staining (Fig. 7B) showed that the cartilage surface of the control group (sham operation) was smooth without regularity or pits. However, the articular cartilage in the PBS- and M1-Abs-treated groups showed pronounced cartilage erosion and cartilage matrix degradation. Interestingly, there were no significant degenerative changes in the M2-Abs-treated group (Fig. 7A, B). Based on these histological findings, we further assessed the cartilage thickness and Mankin scores in each group. Compared with the control (sham operation) group, significantly reduced cartilage thickness and increased Mankin scores were observed in the PBS and M1-ABs groups, while there were no significant differences between the M2-ABs group and the control group (Fig. 7E, F).

Notably, an evaluation of the type distribution of synovial macrophages by immunofluorescence of synovial tissue showed that the positive rates of M2 macrophages in the control (sham operation) group and the M2-Abs group were significantly higher than those in the PBS and M1-ABs groups (Fig. 7C, G). In the PBS and M1-ABs groups, there was an increased percentage of CD86-positive macrophages, indicating that there was increased infiltration of pro-inflammatory M1 macrophages in these synovial tissues, whereas the infiltration of pro-inflammatory macrophages in synovial tissues was largely prevented in the M2-ABs group (Fig. 7D, H). The above results provide further support that M2-derived apoptotic bodies can play an anti-inflammatory role in mice by reprogramming M1 macrophages into M2 macrophages, reducing chondrocyte damage, and thus preventing or alleviating the progression of OA.

Discussion

Persistent inflammation can lead to the onset and progression of chronic inflammatory diseases, such as autoimmune diseases and osteoarthritis.[7] Evidence suggests that the imbalance of M1/M2 caused by the proliferation of M1-Mφs is the main contributor to chronic inflammation.[6] Given the high plasticity between macrophage phenotypes, re-establishing the M1/M2 balance by directly reprogramming M1-Mφs in the inflammatory environment to M2-Mφs may represent an effective strategy for treating chronic inflammatory diseases.[1] Interestingly, the recovery from acute inflammation depends on the clearance of necrotic

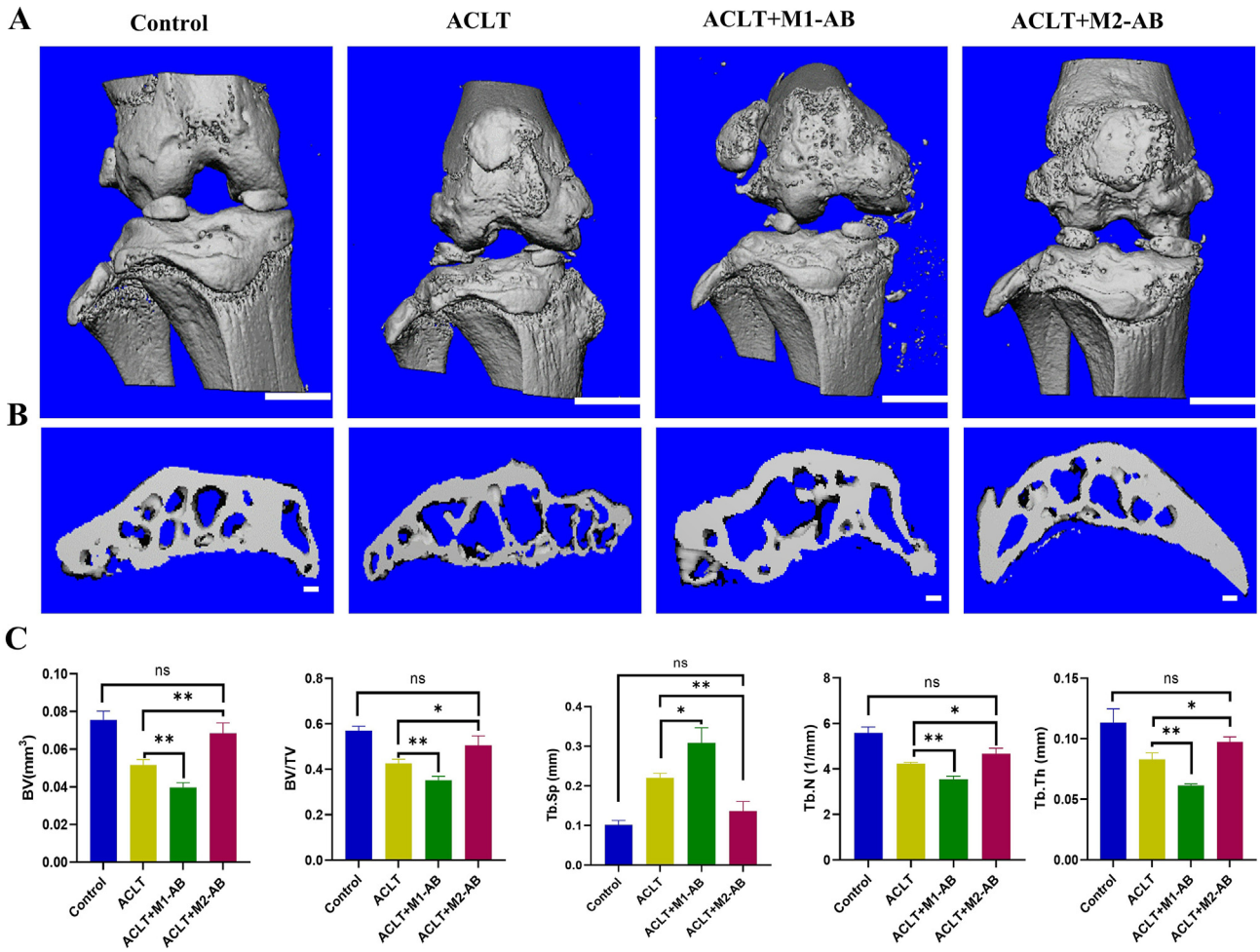

Figure 6 μCT evaluations of M2-ABs treated OA induced by ACLT. **(A)** Three-dimensional μCT images of frontal views of the knee joints at 5 weeks after sham operation or ACLT operation. **(B)** Sagittal views of medial compartment subchondral bone. **(C)** Quantitative analysis of BV, BV/TV, Tb.Sp, Tb.*n* and Tb.Th. *$P < 0.05$, **$P < 0.01$. Scale = 1 mm.

tissue and cell debris by macrophages.[32] Macrophages also play an important role in programmed cell clearance.[33] However, there is no inflammatory response during this process, and evidence suggests that mononuclear phagocytes respond to apoptotic cells by releasing anti-inflammatory factors, including interleukin-10 (IL-10) and TGF-β1, possibly due to the release of biologically active molecules contained in the internalized apoptotic bodies.[34−36] The ABs are extracellular vesicles (1−5 μm) with a submembrane that are considered to be a key mediator of apoptosis.[34,37] Different cell-derived apoptotic corpuscles are loaded with different types of bioactive substances, including microRNA and DNA, to regulate cell-to-cell communication.[38,39]

The accurate delivery of apoptotic bodies to their target cells is a prerequisite for performing apoptosis-mediated cell reprogramming. As noted above, the end-stage clearance of apoptotic cells is mainly accomplished by macrophages. Phosphatidylserine (PtdSer, PS) and annexin-V (Anxin-V) can be transferred to the surface of the vesicle envelope during apoptosis, where they act as signals to trigger phagocytic recognition and uptake.[40] Extracellular vesicles have been shown to be ideal nanomaterials in that they can deliver bioactive substances to target cells without interference from external factors, and thus play a key regulatory role in intercellular communication by regulating target cell function.[41]

Among the microRNAs that were found to be enriched in ABs, some possess the potential to induce the polarization of macrophages towards the M2-Mφs phenotype, which provides a molecular basis for the biological effects of ABs. Among these, miRNA-21 regulates the inflammatory "switch" at an appropriate time and has previously been shown to be positively correlated with the polarization of macrophages towards M2.[42] Considering the abundance of miR-21 found in the M2-ABs in our study (Fig. 4A), we hypothesized that M2-ABs induce macrophage phenotypic reprogramming by delivering miR-21 to M1-Mφs.

In support of this function, we found that M2-ABs-guided M1-to-M2 reprogramming could be significantly reduced by inhibiting miR-21 in M1 macrophages (Fig. 4B, D). In addition, Zhu et al.[43] Found that miR-21−5p was significantly down-regulated in OA chondrocytes, and more importantly, the expression level of miR-21−5p was negatively correlated with cartilage degeneration, which was consistent with the results of this study. Based on these findings, it

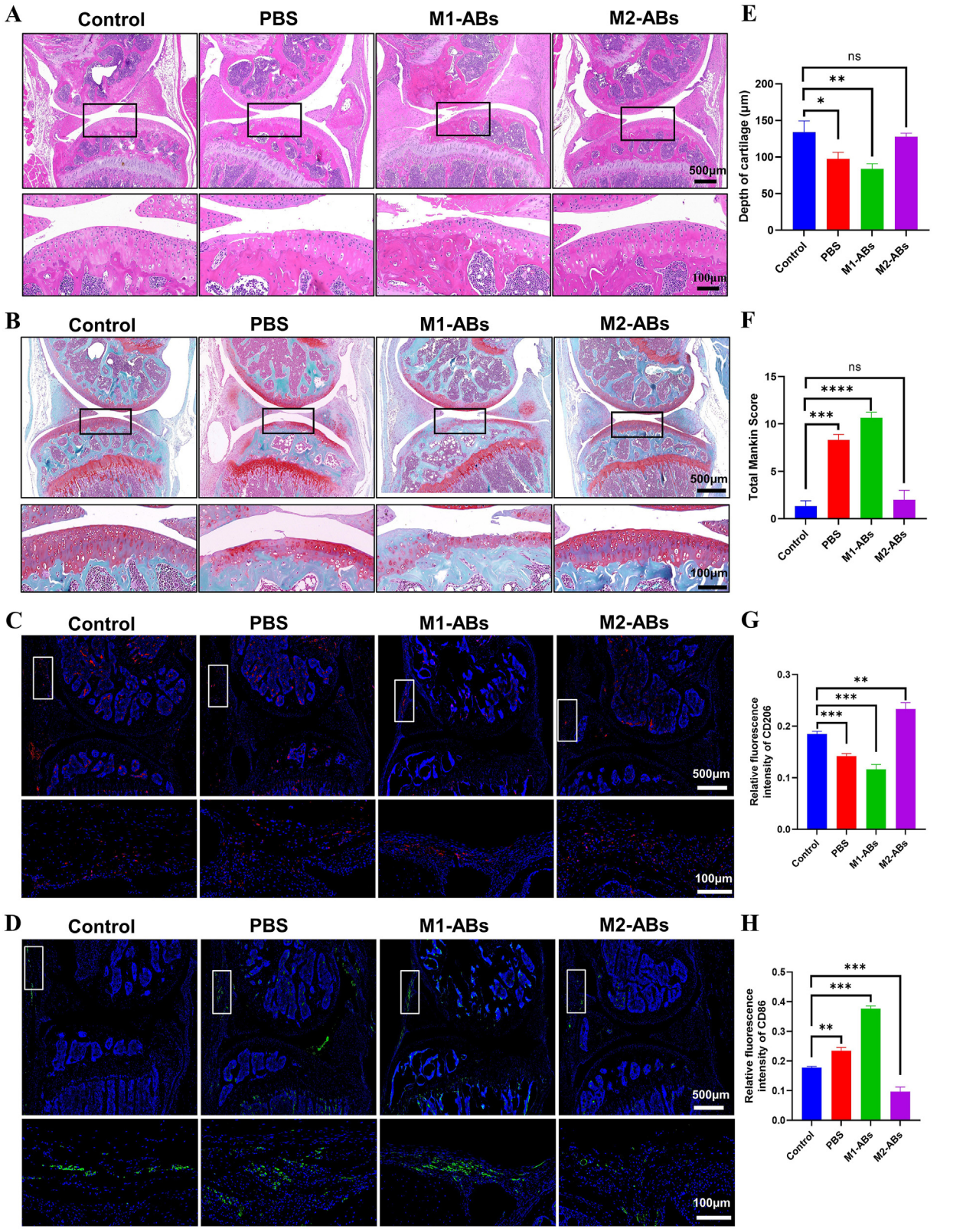

Figure 7 M2-ABs alleviated the disease progression of OA *in vivo* ($n = 5$ for each group). **(A)** Representative images of H&E staining and **(B)** Safranin O-fast green staining from each group. **(C)** Representative immunostaining images of M2 (Arginase, red) and **(D)** M1 (iNOS, green) Mφ in synovial tissues. **(E)** Depth of cartilage. **(F)** Total Mankin scores of articular cartilage. **(G)** Fluorescence intensity analysis of CD206 and **(H)** CD86 in synovial tissue. ***$P < 0.001$, **$P < 0.01$, *$P < 0.05$.

appears that M2-derived ABs have broad regulatory effects on macrophages at the transcriptional level, which contribute to the reprogramming of M1-Mφs to the M2 phenotype in the setting of chronic inflammation associated with OA. This reprogramming leads to rebalancing of the M1/M2 ratio and the prevention or improvement of the inflammatory condition and findings associated with OA.

In this study, we collected ABs derived from M2-Mφs and explored their regulatory role in phenotypic switching in macrophages. We selected OA as the disease model for this study, because a local inflammatory environment in the joint is essential in the development of chondrocyte apoptosis and OA.[44] Such an environment is mainly produced by an imbalance in the polarization of macrophages in the synovial lining.[45,46] M1-derived inflammatory cytokines [including tumor necrosis factor alpha (TNF-α) and interleukin (IL)-1β] lead to increased cartilage apoptosis by promoting the production of stroma-degrading enzymes, whereas M2-Mφs, also known as wound healing macrophages, alter the local inflammatory environment by secreting anti-inflammatory cytokines [primarily IL-4 and IL-10].[47,48] In this study, we found that M2-ABs treatment effectively protected articular cartilage and attenuated early OA development. Following the local injection of apoptotic bodies from M1 and M2 macrophages into the knees of mice with ACLT, it was observed that M2-ABs significantly alleviated the progression of OA and corrected the balance of M1/M2 in situ at an early stage. Although this study indicates that M2-ABs can effectively prevent the progression of OA in mice, the mechanism(s) by which these ameliorate OA has not been fully determined. Therefore, it is necessary to further study the molecular composition and mechanism(s) by which M2-ABs exert their effects. In addition, while we clearly observed that M2-ABs delayed the injury of articular cartilage in animal experiments, the optimal concentration and timing of M2-Abs administered still need to be determined.

Conclusion

To our knowledge, this study is the first demonstration that apoptotic bodies derived from alternatively activated M2-Mφs can alleviate the progression of osteoarthritis by inducing the conversion of classically activated M1-Mφs into a M2-like phenotype. Since M2-ABs guided Mφ reprogramming could effectively correct the imbalance of M1/M2 in OA, we hypothesize that M2-ABs may also provide a promising therapeutic strategy for various diseases related to the imbalance of pro-inflammatory and anti-inflammatory immune responses.

Abbreviations

ACLT	Anterior cruciate ligament transection
BMDM	Bone marrow-derived macrophages
BV	Bone volume
BV/TV	Bone volume/total tissue volume
CCK-8	Cell Counting Kit-8
DLS	Dynamic light scattering
FACS	Fluorescent activated cell sorting
FBS	Fetal bovine serum
HSCs	Hematopoietic stem cells
H&E	Hematoxylin-eosin
ICC	Immunocytochemical
IF	Immunofluorescence
Mφs	Macrophages
NC	Negative control
OA	Osteoarthritis
PBS	Phosphate-buffered saline
q-PCR	Quantitative real-time polymerase chain reaction
RNA-seq	RNA sequencing
ROIs	Region of interests
S&F	Safranin O-fast green
SEM	Scanning electron microscopy
Tb. Sp	Separation
Tb. N	Trabecular number
Tb. Th	Thickness

Ethics declaration

All animal experiments were approved by the Research Ethics Committee of the First Affiliated Hospital of Chongqing Medical University (No. 2021−526).

Author contributions

Wei Huang, Ning Hu and Jun Deng conceived the manuscript. Leilei Qin wrote the first draft. Jianye Yang and Xudong Su revised the first draft. Leilei Qin, Yiting Lei and Xilan li performed the experiments. Lili Dong, Hong Chen, Cheng Chen and Chen Zhao provided grouping suggestions. Huan Zhang provided language and grammar modifications. All authors have read and approved the final manuscript.

Conflict of interests

The authors have no competing interests to disclose.

Funding

This work was supported by the National Natural Science Foundation of China (No. 81972069 and 82072443).

Acknowledgements

Leilei Qin would like to thank Ms. Yuelong Chen for her constant help and support.

Data availability

The datasets used during the current study are available from the corresponding author on reasonable request.

Appendix A. Supplementary data

Supplementary data to this article can be found online at https://doi.org/10.1016/j.gendis.2022.09.010.

References

1. Kim H, Wang SY, Kwak G, et al. Exosome-guided phenotypic switch of M1 to M2 macrophages for cutaneous wound healing. *Adv Sci*. 2019;6(20):1900513.
2. Zhu M. Immunological perspectives on spatial and temporal vaccine delivery. *Adv Drug Deliv Rev*. 2021;178:113966.
3. Rodriguez-Garcia A, Lynn RC, Poussin M, et al. CAR-T cell-mediated depletion of immunosuppressive tumor-associated macrophages promotes endogenous antitumor immunity and augments adoptive immunotherapy. *Nat Commun*. 2021;12(1):877.
4. Rückerl D, Allen JE. Macrophage proliferation, provenance, and plasticity in macroparasite infection. *Immunol Rev*. 2014;262(1):113—133.
5. Wynn TA, Chawla A, Pollard JW. Macrophage biology in development, homeostasis and disease. *Nature*. 2013;496(7446):445—455.
6. Fujisaka S, Usui I, Bukhari A, et al. Regulatory mechanisms for adipose tissue M1 and M2 macrophages in diet-induced obese mice. *Diabetes*. 2009;58(11):2574—2582.
7. Liu S, Li L, Lou P, et al. Elevated branched-chain α-keto acids exacerbate macrophage oxidative stress and chronic inflammatory damage in type 2 diabetes mellitus. *Free Radic Biol Med*. 2021;175:141—154.
8. Ma Y, Yang H, Zong X, et al. Artificial M2 macrophages for disease-modifying osteoarthritis therapeutics. *Biomaterials*. 2021;274:120865.
9. Zhang L, Chen X, Cai P, et al. Reprogramming mitochondrial metabolism in synovial macrophages of early osteoarthritis by a camouflaged meta-defensome. *Adv Mater*. 2022;34(30):e2202715.
10. Chu SY, Chou CH, Huang HD, et al. Mechanical stretch induces hair regeneration through the alternative activation of macrophages. *Nat Commun*. 2019;10(1):1524.
11. Miyazaki T, Tonami K, Hata S, et al. Calpain-6 confers atherogenicity to macrophages by dysregulating pre-mRNA splicing. *J Clin Invest*. 2016;126(9):3417—3432.
12. Abels ER, Breakefield XO. Introduction to extracellular vesicles: biogenesis, RNA cargo selection, content, release, and uptake. *Cell Mol Neurobiol*. 2016;36(3):301—312.
13. Bergsmedh A, Szeles A, Henriksson M, et al. Horizontal transfer of oncogenes by uptake of apoptotic bodies. *Proc Natl Acad Sci U S A*. 2001;98(11):6407—6411.
14. Lötvall J, Hill AF, Hochberg F, et al. Minimal experimental requirements for definition of extracellular vesicles and their functions: a position statement from the International Society for Extracellular Vesicles. *J Extracell Vesicles*. 2014;3:26913.
15. Nawaz M, Fatima F, Vallabhaneni KC, et al. Extracellular vesicles: evolving factors in stem cell biology. *Stem Cells Int*. 2016;2016:1073140.
16. Merchant ML, Rood IM, Deegens JKJ, et al. Isolation and characterization of urinary extracellular vesicles: implications for biomarker discovery. *Nat Rev Nephrol*. 2017;13(12):731—749.
17. Battistelli M, Falcieri E. Apoptotic bodies: particular extracellular vesicles involved in intercellular communication. *Biology*. 2020;9(1).
18. Zheng C, Sui B, Zhang X, et al. Apoptotic vesicles restore liver macrophage homeostasis to counteract type 2 diabetes. *J Extracell Vesicles*. 2021;10(7):e12109.
19. Poon IK, Lucas CD, Rossi AG, et al. Apoptotic cell clearance: basic biology and therapeutic potential. *Nat Rev Immunol*. 2014;14(3):166—180.
20. Woo CH, Kim HK, Jung GY, et al. Small extracellular vesicles from human adipose-derived stem cells attenuate cartilage degeneration. *J Extracell Vesicles*. 2020;9(1):1735249.
21. Moon SJ, Woo YJ, Jeong JH, et al. Rebamipide attenuates pain severity and cartilage degeneration in a rat model of osteoarthritis by downregulating oxidative damage and catabolic activity in chondrocytes. *Osteoarthritis Cartilage*. 2012;20(11):1426—1438.
22. Navegantes KC, de Souza Gomes R, Pereira PAT, et al. Immune modulation of some autoimmune diseases: the critical role of macrophages and neutrophils in the innate and adaptive immunity. *J Transl Med*. 2017;15(1):36.
23. Zhang H, Lin C, Zeng C, et al. Synovial macrophage M1 polarisation exacerbates experimental osteoarthritis partially through R-spondin-2. *Ann Rheum Dis*. 2018;77(10):1524—1534.
24. Dou G, Tian R, Liu X, et al. Chimeric apoptotic bodies functionalized with natural membrane and modular delivery system for inflammation modulation. *Sci Adv*. 2020;6(30):eaba2987.
25. Shi Y, Ma J, Zhang X, et al. Hypoxia combined with spheroid culture improves cartilage specific function in chondrocytes. *Integr Biol (Camb)*. 2015;7(3):289—297.
26. Valadi H, Ekström K, Bossios A, et al. Exosome-mediated transfer of mRNAs and microRNAs is a novel mechanism of genetic exchange between cells. *Nat Cell Biol*. 2007;9(6):654—659.
27. Neaga A, Bagacean C, Tempescul A, et al. MicroRNAs associated with a good prognosis of acute myeloid leukemia and their effect on macrophage polarization. *Front Immunol*. 2020;11:582915.
28. Squadrito ML, Etzrodt M, De Palma M, et al. MicroRNA-mediated control of macrophages and its implications for cancer. *Trends Immunol*. 2013;34(7):350—359.
29. Wei Y, Schober A. MicroRNA regulation of macrophages in human pathologies. *Cell Mol Life Sci*. 2016;73(18):3473—3495.
30. Burr DB, Gallant MA. Bone remodelling in osteoarthritis. *Nat Rev Rheumatol*. 2012;8(11):665—673.
31. Bapat S, Hubbard D, Munjal A, et al. Pros and cons of mouse models for studying osteoarthritis. *Clin Transl Med*. 2018;7(1):36.
32. Westman J, Grinstein S, Marques PE. Phagocytosis of necrotic debris at sites of injury and inflammation. *Front Immunol*. 2019;10:3030.
33. Liu G, Wu C, Wu Y, et al. Phagocytosis of apoptotic cells and immune regulation. *Scand J Immunol*. 2006;64(1):1—9.
34. Atkin-Smith GK, Poon IKH. Disassembly of the dying: mechanisms and functions. *Trends Cell Biol*. 2017;27(2):151—162.
35. Atkin-Smith GK, Tixeira R, Paone S, et al. A novel mechanism of generating extracellular vesicles during apoptosis via a beads-on-a-string membrane structure. *Nat Commun*. 15 2015;6:7439.
36. Förtsch D, Röllinghoff M, Stenger S. IL-10 converts human dendritic cells into macrophage-like cells with increased antibacterial activity against virulent Mycobacterium tuberculosis. *J Immunol*. 2000;165(2):978—987.
37. Akers JC, Gonda D, Kim R, et al. Biogenesis of extracellular vesicles (EV): exosomes, microvesicles, retrovirus-like vesicles, and apoptotic bodies. *J Neuro Oncol*. 2013;113(1):1—11.
38. Holmgren L, Szeles A, Rajnavölgyi E, et al. Horizontal transfer of DNA by the uptake of apoptotic bodies. *Blood*. 1999;93(11):3956—3963.
39. Zernecke A, Bidzhekov K, Noels H, et al. Delivery of microRNA-126 by apoptotic bodies induces CXCL12-dependent vascular protection. *Sci Signal*. 2009;2(100):ra81.
40. Segawa K, Nagata S. An apoptotic "eat me" signal: phosphatidylserine exposure. *Trends Cell Biol*. 2015;25(11):639—650.
41. Barile L, Moccetti T, Marbán E, et al. Roles of exosomes in cardioprotection. *Eur Heart J*. 2017;38(18):1372—1379.
42. Lu J, Xie L, Sun S. The inhibitor miR-21 regulates macrophage polarization in an experimental model of chronic obstructive pulmonary disease. *Tob Induc Dis*. 2021;19:69.

43. Zhu H, Yan X, Zhang M, et al. miR-21-5p protects IL-1β-induced human chondrocytes from degradation. *J Orthop Surg Res*. 2019;14(1):118.
44. Zhang H, Cai D, Bai X. Macrophages regulate the progression of osteoarthritis. *Osteoarthritis Cartilage*. 2020;28(5):555—561.
45. Griffin TM, Scanzello CR. Innate inflammation and synovial macrophages in osteoarthritis pathophysiology. *Clin Exp Rheumatol*. 2019;37(5):57—63.
46. O'Brien K, Tailor P, Leonard C, et al. Enumeration and localization of mesenchymal progenitor cells and macrophages in synovium from normal individuals and patients with pre-osteoarthritis or clinically diagnosed osteoarthritis. *Int J Mol Sci*. 2017;18(4).
47. Dai M, Sui B, Xue Y, et al. Cartilage repair in degenerative osteoarthritis mediated by squid type II collagen via immunomodulating activation of M2 macrophages, inhibiting apoptosis and hypertrophy of chondrocytes. *Biomaterials*. 2018;180:91—103.
48. Harrell CR, Markovic BS, Fellabaum C, et al. Mesenchymal stem cell-based therapy of osteoarthritis: current knowledge and future perspectives. *Biomed Pharmacother*. 2019;109:2318—2326.